Geochemical Perspectives Letters EAG

H-N budgets and isotopic signatures of Oued Chebeika 002 and CI reservoir heterogeneity

Y. Marrocchi, E. Füri, L. Zimmermann, L. Piani

Supplementary Information

The Supplementary Information includes:

- Analytical Methods (H, N and Noble Gases)
- Noble Gas (Ne, Ar) Isotopic Composition of OC 002
- Nitrogen Concentration and Isotopic Composition of OC 002 – Step-heating Profiles
- δD *vs.* C and δD *vs.* C/H Diagrams for CI and CM Chondrites
- Figures S-1 to S-5
- Tables S-1 to S-3
- Supplementary Information References

Analytical Methods (H, N and Noble Gases)

The hydrogen concentration, [H], and isotopic composition, D/H, of one OC 002 aliquot (1.21 mg) was determined on-line using the Thermo Scientific EA IsoLink - deltaV IRMS System at the stable isotope mass spectrometry facility of the Centre de Recherches Pétrographiques et Géochimiques (CRPG, Nancy, France) according to the procedure developed by Lupker *et al.* (2012) for Himalayan sediments and slightly modified for measuring meteorites (Marrocchi *et al.*, 2020, 2021; Vacher *et al.*, 2020). First, the meteoritic sample was crushed into powder in an agate mortar, weighed in a tin capsule, and then the sample and capsule were loaded into a sample carousel and degassed under vacuum at 120 °C for 48 h in a degassing canister (Lupker *et al.*, 2012); degassing for less than 48 h has been shown to result in increased variability of water contents and H isotopic compositions due to residual adsorbed water (Lupker *et al.*, 2012). After dehydration, the degassing canister was opened in a dry, N_2-flushed glove box, and the sample carousel was transferred into a sealed auto-sampler initially pre-flushed with He. The auto-sampler was then connected to the EA and pumped out during 20 min before being opened to the reduction column, a precautionary step to prevent potential rehydration of the samples in the event of atmospheric exposure between degassing and analysis.

The sample was combusted at 1450 °C (the temperature required to ensure rapid sample reduction and to prevent any CH_3 formation) in a glassy carbon reaction tube filled with glassy carbon chips and itself placed into a ceramic liner to reduce hydroxyls (OH) released by the samples into H_2, according to the reaction: 2OH + C (unlimited in reactor) → 2CO + H_2. The produced gases were separated on a chromatographic column maintained at 60 °C, and the extracted H_2 was introduced into the mass spectrometer through an open-split, and its D/H isotopic composition was analysed. The extracted H_2 was corrected for H_3^+ contributions using in-house H_2 standard injections, and [H] and D/H were determined by comparison with seven internal standards routinely included during the analyses: (i) phlogopite (Mica-Mg, 0.29 wt.% H, D/H = 143.8 × 10^{-6}), (ii) muscovite (MuscD65, 0.474 wt.% H, D/H = 142.6 × 10^{-6}), (iii) a fine-grained marine sediment from the Bay of Bengal (SO188, 0.489 wt.% H, D/H = 142.7 × 10^{-6}), and (iv) four basalts with different H concentrations (CYP78, 0.14 wt.% H; JB3-GSJ, 0.20 wt.% H; SR2-02, 0.27 wt.% H; and GMR-KS12, 0.42 wt.% H). Uncertainties on H concentrations and isotopic compositions were estimated by accounting for both internal measurement errors and external reproducibility of the standards. Hydrogen isotopic compositions are reported as D/H ratios or as δD values (‰) relative to VSMOW. The reproducibility of this method is better than 15% (2σ) for [H] and 0.5 × 10^{-6} for D/H (or 5‰ for δD). The hydrogen concentration and isotopic composition of the OC 002 aliquot is available at https://doi.org/10.24396/ORDAR-201.

Noble gases (Ne, Ar) and N were extracted from OC 002 fragments at CRPG's noble gas facility using established static-vacuum laser-heating protocols previously applied to Hayabusa2 (Broadley *et al.*, 2023; Okazaki *et al.*, 2023; Gamblin *et al.*, 2024) and OSIRIS-REx samples (Marty *et al.*, 2026). Six fragments (0.048 to 0.417 mg) were weighed using a Mettler Toledo XPR2U™ microbalance and then loaded into individual pits of a Zn-Se-windowed laser chamber. The sample pits were covered with a second ZnSe window to prevent the small meteorite fragments from bouncing out of position during laser heating and degassing. The laser chamber was then connected to the purification line of the Noblesse–HR noble gas mass spectrometer, pumped to ultra-high vacuum (~10^{-9} Torr), and baked at ~100 ºC overnight. Gas release was achieved using a continuous-wave 10.6 µm CO_2 laser (MIR10^2, Elemental Scientific), either in a single step or in 8–11 increments (1 to 100 % of 32 W), with heating monitored via a CCD camera. A limitation of this method is the lack of knowledge of the sample's temperature at any given laser power.

The extracted gases were split into two calibrated volumes for separate purification of noble gases and N, following Zimmermann and Füri (2015) and Zimmermann *et al.* (2015). Noble gases were purified in an all-metal line using a Ti sponge and two SAES™ Ti-Al getters, with Ar separated from Ne by cryogenic trapping on a charcoal finger at –196 °C. Nitrogen was purified within a Pyrex–quartz-glass line: reactive species were oxidized by O_2 released from heated CuO sticks (450–900 °C); the resulting oxides were trapped at –180 °C, while NO_X remained in the gas phase and was subsequently reduced to N_2 by stepwise CuO cooling (900–300 °C). Additional Pt foils, held at –175 °C, trapped remaining impurities (*e.g.*, H_2O, CO_2, C_xH_y). Before analysis, the gas pressure was checked with an ion gauge; if necessary, the N_2 amount was adjusted by volume dilution to match purified air standards.

Ne-Ar-N_2 abundances and isotope ratios were determined sequentially on the 3F4M Noblesse–HR noble gas mass spectrometer (Nu Instruments) at a trap current of 150 µA (Zimmermann *et al.*, 2025). Source and zoom optics settings were tuned for each gas to optimise sensitivity and minimise mass bias, and to achieve high mass resolution (~700) and mass resolving power (~7000), respectively. Neon isotopes were measured simultaneously on ion counters ($^{22}Ne^+$ on IC0, $^{21}Ne^+$ on IC2, $^{20}Ne^+$ on IC3), with peak-jumping to $^{44}CO_2^+$ (IC0), over 25 cycles. Contributions from $^{40}Ar^{2+}$ and $^{44}CO_2^{2+}$ were minimized with cryogenic trapping and getters. The $^{22}Ne^+$ signal was corrected using a measured $^{44}CO_2^{2+}/^{44}CO_2^+$ ionisation ratio of 0.55 %; owing to the low Ne amounts analysed and elevated $^{44}CO_2^+$ signals (~1000–2000 cps) observed during some heating steps, this correction amounted to 1–11 cps. Argon isotopes were analysed in multi-collection mode ($^{40}Ar^+$ on Fa0 [10^{11} Ω], $^{38}Ar^+$ on IC2, $^{36}Ar^+$ on IC3). N_2 isotopologues were also measured simultaneously ($^{14}N^{14}N^+$ on Fa2 [10^{11} Ω], $^{14}N^{15}N^+$ on Fa1 [10^{12} Ω], and $^{15}N^{15}N^+$ on IC0), with $^{12}C^{16}O^+$ monitored for CO correction, and $^{13}C^{16}O^+$ and $^{12}C^{18}O^+$ interferences estimated from natural isotopic abundances. Baseline- and interference-corrected Ne, Ar, and N_2 ion signals, as well as $^{20}Ne/^{22}Ne$, $^{21}Ne/^{22}Ne$, $^{40}Ar/^{36}Ar$, $^{38}Ar/^{36}Ar$, $^{28}N_2/^{29}N_2$, and $^{29}N_2/^{30}N_2$ ratios, extrapolated to $t = 0$, are available for download at https://doi.org/10.24396/ORDAR-205.

Procedural blanks (with the laser off), measured prior to the sample analyses, averaged 4.4 ± 0.8 × 10^{-16} mol ^{20}Ne, 2.34 ± 0.04 × 10^{-17} mol ^{36}Ar, 9.2 ± 0.3 × 10^{-13} mol $^{28}N_2$. Sensitivity (4.3 ± 0.3 × 10^{-5} A/Torr for ^{20}Ne, 2.18 ± 0.03 × 10^{-4} A/Torr for ^{36}Ar, and 1.39 ± 0.06 × 10^{-4} A/Torr for $^{28}N_2$, on average) and instrumental mass fractionation were assessed via repeated analyses of purified air standard aliquots. All abundances and isotope ratios were corrected for blanks, sensitivity, and instrumental mass fractionation (see Gamblin *et al.*, 2024, for details). Nitrogen isotopic compositions are reported in $\delta^{15}N$ notation, calculated for N_2 as $\delta^{15}N$ (‰) = $\{[1 + 2 \times (^{28}N_2/^{29}N_2)_{atm}] - [1 + 2 \times (^{28}N_2/^{29}N_2)_{measured}] - 1\} \times 1000$, where $(^{28}N_2/^{29}N_2)_{atm}$ is the isotopic composition of atmospheric N_2 (136.05; Nier, 1950). Analytical reproducibility of air standard $^{28}N_2/^{29}N_2$ ratios was ±0.9 ‰ (1 σ), with negligible contribution from analytical precision. Calculated Ne, Ar, and N_2 concentrations (per initial sample mass) and isotope ratios are available for download at https://doi.org/10.24396/ORDAR-205.

Noble Gas (Ne, Ar) Isotopic Composition of OC 002

Due to the small sample sizes analysed here (≪1 mg), blank contributions to the measured ^{20}Ne abundances exceeded 30 % for all steps during the step-heating analyses of three OC 002 fragments. Only the single-step heating analyses of three additional fragments allowed assessment of the Ne isotopic composition of OC 002 (Fig. S-1). The results are consistent with those obtained for other CI chondrites: Ne consists of a mixture between a presolar component mainly hosted by nanodiamonds (so-called Ne-HL or Ne-P3) and cosmogenic Ne produced by spallation reactions induced by the interaction with galactic cosmic rays (GCR). Given that several CI samples, including two OC 002 fragments, have Ne isotopic compositions below the expected HL-GCR mixing line, a contribution from Ne–G,R—a nucleosynthetic, pure ^{22}Ne endmember hosted by presolar SiC and graphite—cannot be ruled out. In contrast, many samples returned from the asteroids Ryugu (Nakamura *et al*., 2022; Broadley *et al*., 2023; Meshik *et al*., 2023; Okazaki *et al*., 2023; Gamblin *et al*., 2024) and Bennu (Barnes *et al*., 2025; Marty *et al*., 2026) contain a significant proportion of implanted solar wind (SW) Ne, indicating that they were irradiated by the SW at the surface of these airless asteroids.

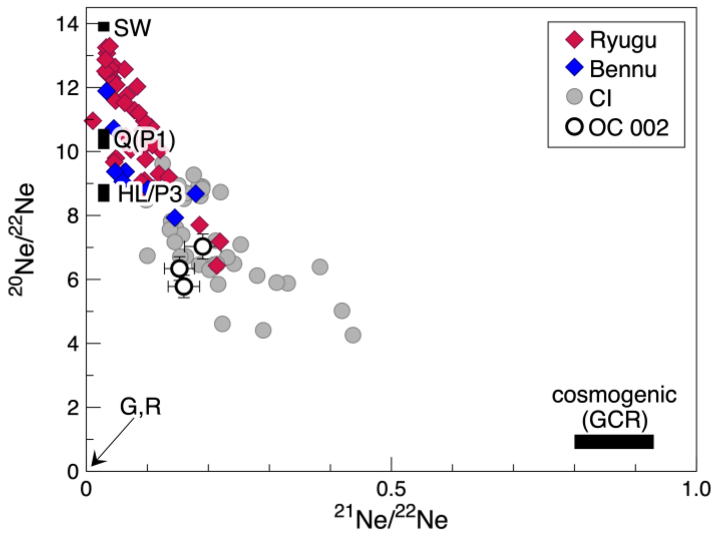

Figure S-1 Neon isotopic composition of OC 002, determined by single-step heating of three fragments, compared with that of samples returned from Ryugu (Nakamura *et al*., 2022; Okazaki *et al*., 2023; Broadley *et al*., 2023; Meshik *et al*., 2023; Gamblin *et al*., 2024) and Bennu (Barnes *et al*., 2025; Marty *et al*., 2026), as well as other CI chondrite samples (Schultz and Franke, 2004, and references therein; Nakamura *et al*., 2022; Patzek *et al*., 2025). Endmember values are from Ott (2014).

In the case of Ar, all but the first heating step of the three step-heating analyses (conducted at the lowest laser power of 1 %), yielded $^{38}Ar^+$ and $^{36}Ar^+$ signals well above blank levels, giving an average ^{38}Ar/^{36}Ar ratio of 0.187 ± 0.003 for the six OC 002 fragments. This value agrees, within analytical uncertainty, with that of Ar-Q (0.1874 ± 0.0004; Busemann *et al*., 2000), supporting the interpretation that the so-called phase Q (also labelled P1 in the literature) is the dominant carrier of Ar in CI-like material (Marty *et al*., 2026, and references therein).

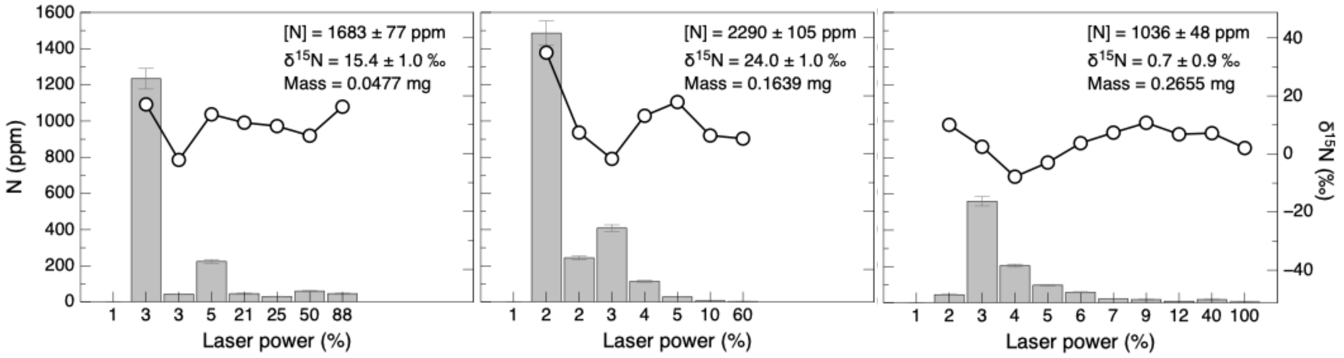

Figure S-2 Nitrogen abundance (grey bars, left *Y* axis) and isotopic composition (open circles, right *Y* axis) of three OC002 fragments as a function of laser power (1 to 100 % of 32 W). Abundances are given as parts per million (ppm weight).

Nitrogen Concentration and Isotopic Composition of OC 002 – Step-heating Profiles

Bulk data are provided in Table S-1. Figure S-2 shows the N concentrations and isotopic compositions of three OC 002 fragments, determined by gradually increasing the power of the CO_2 laser in 8–11 increments (1 to 100 % of 32 W). The amount of N released during the first step (1 %) was comparable to the blank level. The step-heating profiles reveal that N is predominantly released at low temperature (*i.e.* at low laser power of 2–3 %). The summed N concentrations (1036 ± 48 to 2290 ± 105 ppm) fall within the range of previously published values for CI chondrites (944 ± 25 ppm to 0.24 wt%; see compiled data at https://doi.org/10.24396/ORDAR-190), excluding two exceptionally high values of 0.56 and 0.82 wt% reported for Orgueil by Pearson *et al.* (2006). The $\delta^{15}N$ values vary between –7.8 ± 1.3 and +34.9 ± 1.4 ‰ in individual steps. Abundance-weighted averages range from 0.7 ± 0.9 to 24.0 ± 1.0 ‰, and are consistent with the values of +1.5 ± 1.3 ‰ and +27.4 ± 1.4 ‰ obtained by single-step heating of two additional OC 002 fragments (see main text).

Table S-1 Bulk values measured for the six aliquots: ^{22}Ne (mol g^{-1}), $^{20}Ne/^{22}Ne$ and $^{21}Ne/^{22}Ne$ ratios, ^{36}Ar (mol g^{-1}), $^{38}Ar/^{36}Ar$ and $^{40}Ar/^{36}Ar$ ratios, nitrogen concentration (N, ppm), and nitrogen isotopic composition ($\delta^{15}N$).

Sample	Mass	# of heating steps	^{22}Ne	+/-	$^{20}Ne/^{22}Ne$	+/-	$^{21}Ne/^{22}Ne$	+/-	^{36}Ar	+/-	$^{38}Ar/^{36}Ar$	+/-	N	+/-	$\delta^{15}N$	+/-
	mg		mol/g	1σ		1σ		1σ	mol/g	1σ		1σ	ppm	1σ	‰	1σ
OUED6	0.0477	8	b.d.						7.80E-11	1.24E-12	0.187	0.003	1683	77	15.4	1.0
OUED5	0.2655	11	b.d.						4.36E-11	6.60E-13	0.189	0.003	1036	48	0.7	0.9
OUED1	0.1639	8	b.d.						4.99E-11	7.56E-13	0.187	0.003	2290	105	24.0	1.0
OUED2	0.1768	1	1.55E-12	1.29E-13	6.34	0.37	0.1526	0.0246	5.04E-11	7.44E-13	0.188	0.001	n.d.		n.d.	
OUED7	0.1266	1	2.05E-12	1.72E-13	5.78	0.35	0.1599	0.0258	5.87E-11	8.67E-13	0.188	0.001	1009	46	1.5	1.3
OUED3	0.4170	1	1.25E-12	1.03E-13	7.03	0.39	0.1909	0.0300	5.13E-11	7.54E-13	0.189	0.001	1494	68	27.4	1.4

b.d. Below detection, i.e., blank contribution >30% for all heating steps.
n.d. Not determined

δD *vs.* C and δD *vs.* C/H Diagrams for CI and CM Chondrites

Figure S-3 shows the H isotopic compositions of CI and CM chondrites as a function of their respective C contents and C/H ratios.

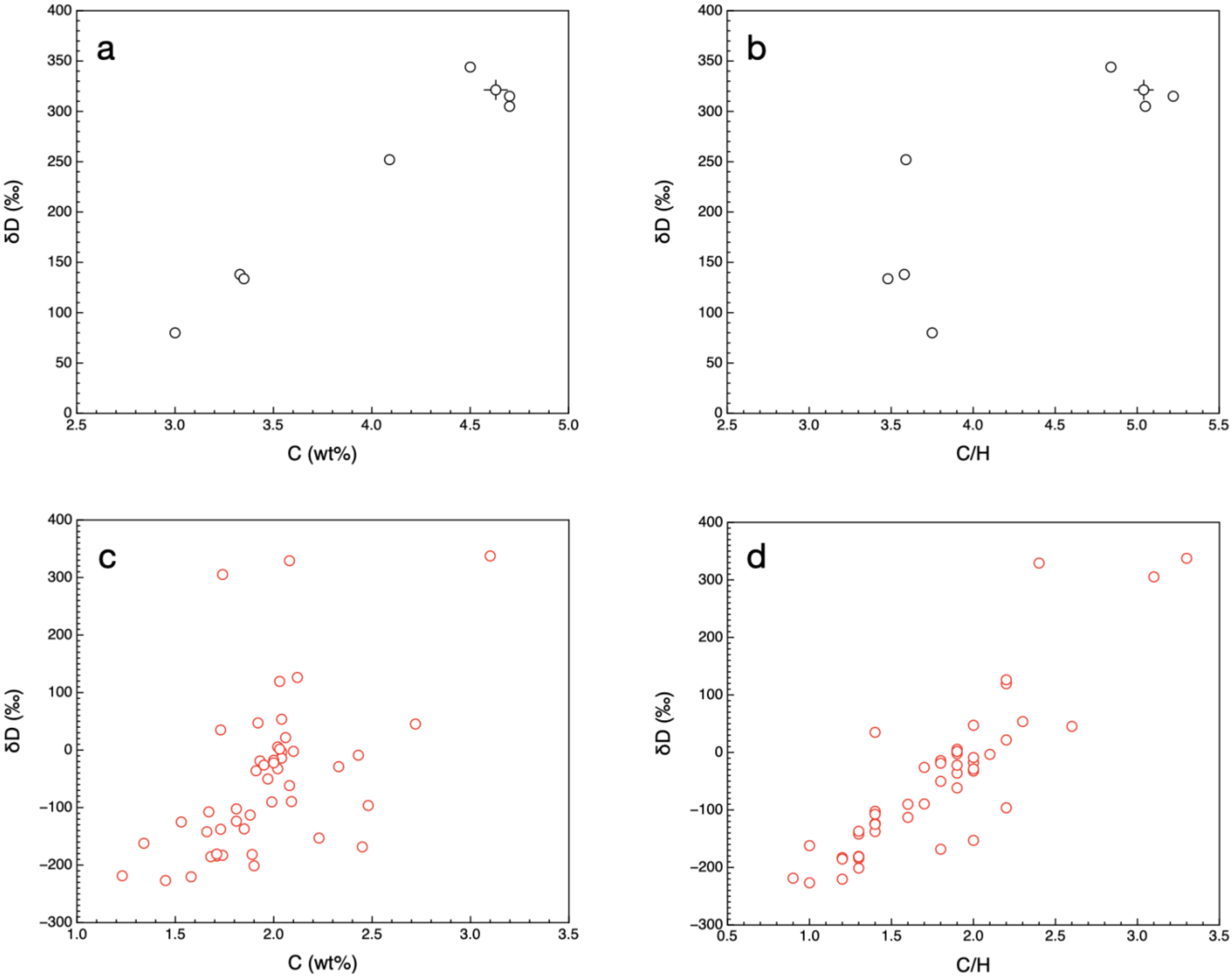

Figure S-3 **(a)** δD as a function of the C content in different CI, Bennu, and Ryugu samples. **(b)** δD as a function of the C/H ratios in different CI, Bennu, and Ryugu samples (data from this study; Vacher *et al*., 2020; Nakamura *et al*., 2022; Yokoyama *et al*., 2023; Lauretta *et al*., 2024; data are reported in Table S-2). **(c)** δD as a function of the C content in CM chondrites. **(d)** δD as a function of the C/H ratios in CM chondrites (data from Alexander *et al*., 2012 and reported in Table S-3).

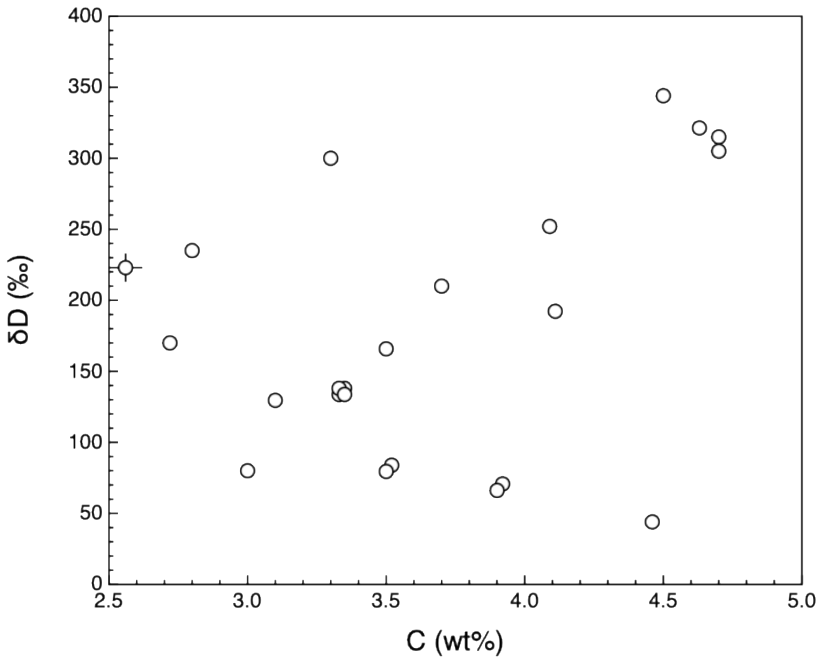

Figure S-4 δD as a function of the C content in CIs (see Table S-2 and compiled data at https://doi.org/10.24396/ORDAR-225).

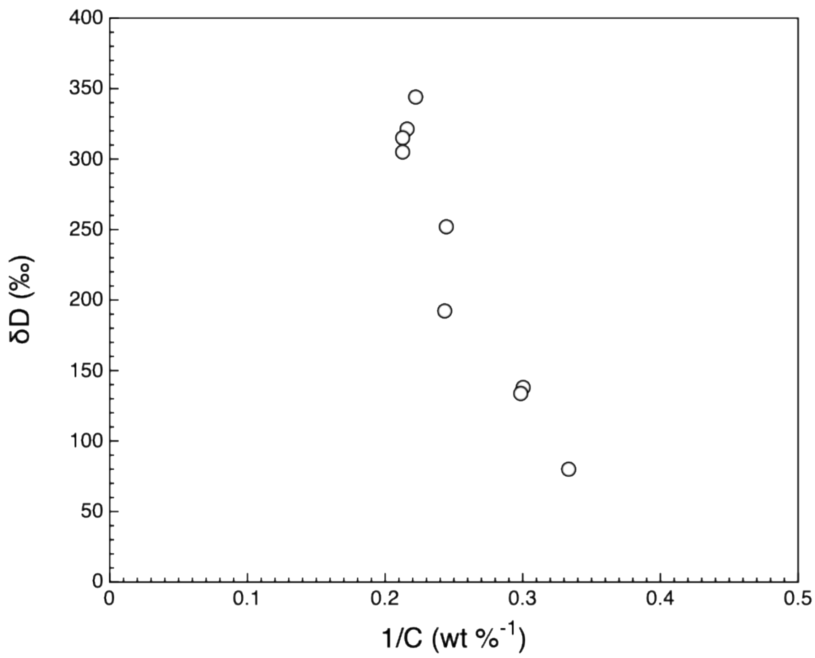

Figure S-5 δD as a function of the 1/C ratios of the CIs reported in Fig. S-3 (data from this study; Vacher *et al.*, 2020; Nakamura *et al.*, 2022; Yokoyama *et al.*, 2023; Lauretta *et al.*, 2024). See Table S-2 and compiled data at https://doi.org/10.24396/ORDAR-225.

Table S-2 δD values, C contents and C/H ratios in different CI, Bennu, and Ryugu samples for all samples reported in Fig. S-3 (data from this study; Vacher *et al*., 2020; Nakamura *et al*., 2022; Yokoyama *et al*., 2023; Lauretta *et al*., 2024).

	δD	err	C	err	C/H	err
Orgueil	138	1.5	3.33		3.58	
Alais	133.7	1.5	3.35		3.48	
OC 002	81.2	2	3		3.75	
Ryugu	321.33	10	4.63	0.06	5.04	0.08
	252		4.09		3.59	
Bennu	315	2	4.7		5.22	
	305		4.7		5.05	
	344		4.5		4.84	

Table S-3 δD values, C contents and C/H ratios for all CM reported in Fig. S-3 (data from Alexander *et al*., 2012).

	δD (‰)	1σ	C (wt%)	1σ	C/H
ALHA 81002 H	-142.0	1.8	1.66		1.27
ALH 83100 H	-201.1	0.5	1.90		1.30
ALH 84029	-184.1	2.5	1.71		1.26
ALH 84034	-182.9	2.9	1.74		1.24
ALH 84042	-185.3	0.5	1.68		1.24
ALH 84044	-180.7	1.9	1.71		1.28
ALH 85013	-137.6	0.5	1.73	0.05	1.43
Banten	-32.4	0.8	2.02		1.98
Cold Bokk H	-168.3	0.3	2.45		1.81
DNG 06004	-3.4	1.1	2.04		2.07
DOM 08003	-137.0	11.1	1.85		1.26
DOM 08013	47.2	2.4	1.92		2.00
EET 96006	-90.1	0.6	1.99		1.56
EET 96016	-89.5	0.1	2.09		1.68
GRA 98074	-14.1	4.3	2.04		1.83
GRO 95566	-18.8	1.1	1.93		1.75
LAP 02239	-36.0	0.7	1.91		1.87
LAP 02333	-2.2	4.6	2.10		1.85
LAP 02336	5.5	2.3	2.02		1.91
LAP 03718	1.7	3.6	2.03		1.90
LAP 03785	-123.6	0.8	1.81		1.41
LEW 85311	119.4	2.9	2.03		2.23
LEW 85312	126.3	4.1	2.12		2.24
LEW 87016	-26.0	2.0	1.95		1.72
LEW 87022	-112.9	2.4	1.88		1.57
LEW 87148	-102.2	4.5	1.81		1.43
LEW 88001	-50.2	0.0	1.97		1.78
LEW 90500	-95.4	2.9	1.84	0.04	1.69
LON 94102	21.7	0.7	2.06	0.05	2.21
MAC 88101	35.0	5.1	1.73	0.01	1.44
MAC 88176	-107.4	2.7	1.67		1.39
MCY 05230	-17.6	3.7	2.00		2.03
MET 00432	45.3	0.2	2.72	0.02	2.56
MET 01070 H	-220.3	0.0	1.58		1.16
Mighei H	-96.3	0.2	2.48		2.20
Murchison	-61.7	3.1	2.08		1.94
Murray H	-28.8	3.2	2.33		2.01
Nagoya II	-181.5	1.0	1.89	0.11	1.34
Nogoya H	-152.9	0.7	2.23		2.01
QUE 97990 H	-22.2	1.0	2.00		1.91
QUE 99355	-125.0	2.3	1.53	0.01	1.36
SCO 06014	-162.0	2.0	1.34		1.01
SCO 06043 H	-226.7	0.0	1.45		1.04
SCO 06043 II	-218.6	4.0	1.23		0.92
TIL 91722	53.7	0.7	2.04		2.25
Y 791198 H	-8.9	1.0	2.43		2.01

Supplementary Information References

Alexander, C.M.O'D., Bowden, R., Fogel, M.L., Howard, K.T., Herd, C.D.K., Nittler, L.R. (2012) The Provenances of Asteroids, and Their Contributions to the Volatile Inventories of the Terrestrial Planets. *Science* 337, 721–723, https://doi.org/10.1126/science.1223474

Barnes, J.J., Nguyen, A.N., Abernethy, F.A.J., Bajo, K., Bekaert, D.V. *et al.* (2025) The variety and origin of materials accreted by Bennu's parent asteroid. *Nature Astronomy* 9, 1785–1802. https://doi.org/10.1038/s41550-025-02631-6

Broadley, M.W., Byrne, D.J., Füri, E., Zimmermann, L., Marty, B. *et al.* (2023) The noble gas and nitrogen relationship between Ryugu and carbonaceous chondrites. *Geochimica et Cosmochimica Acta* 345, 62–74. https://doi.org/10.1016/j.gca.2023.01.020

Busemann, H., Baur, H., Wieler, R. (2000) Primordial noble gases in "phase Q" in carbonaceous and ordinary chondrites studied by closed-system stepped etching. *Meteoritics & Planetary Science* 35, 949–973. https://doi.org/10.1111/j.1945-5100.2000.tb01485.x

Gamblin, J., Füri, E., Marty, B., Zimmermann, L., Bekaert, D.V. (2024) Dissecting the complex Ne-Ar-N signature of asteroid Ryugu by step-heating analysis. *Geochemical Perspectives Letters* 31, 44–48. https://doi.org/10.7185/geochemlet.2431

Lauretta, D.S., Connolly Jr, H.C, Aebersold, J.E., Alexander, C.M.O'D., Ballouz, R.-L. *et al.* (2024) Asteroid (101955) Bennu in the laboratory: Properties of the sample collected by OSIRIS-REx. *Meteoritics & Planetary Science* 59, 2453–2486. https://doi.org/10.1111/maps.14227

Lupker, M., France-Lanord, C., Galy, V., Lavé, J., Gaillardet, J. *et al.* (2012) Predominant floodplain over mountain weathering of Himalayan sediments (Ganga basin). *Geochimica et Cosmochimica Acta* 84, 410–432. https://doi.org/10.1016/j.gca.2012.02.001

Marrocchi, Y., Bonal, L., Gattacceca, J., Piani, L., Beck, P. *et al.* (2020) The Piancaldoli meteorite: A forgotten primitive LL3.10 ordinary chondrite. *Meteoritics & Planetary Science* 55, 1924–1935. https://doi.org/10.1111/maps.13552

Marrocchi, Y., Avice, G., Barrat, J.-A. (2021) The Tarda Meteorite: A Window into the Formation of D-type Asteroids. *The Astrophysical Journal Letters* 913, L9. https://doi.org/10.3847/2041-8213/abfaa3

Marty B., Zimmermann, L., Füri, E., Bekaert, D.V., Barnes, J.J., Nguyen, A.N., Connolly, H.C., Lauretta, D.S. (2026) Noble gases and nitrogen in material from asteroid Bennu. *Meteoritics & Planetary Science* (in press). https://doi.org/10.1111/maps.70058

Meshik, A., Pravdivtseva, O., Okazaki, R., Yogata, K., Yada, T. *et al.* (2023) Noble gas mass-spectrometry for extraterrestrial micro-samples: analyses of asteroid matter returned by Hayabusa2 JAXA mission. *Journal of Analytical Atomic Spectrometry* 38, 1785–1797. https://doi.org/10.1039/D3JA00125C

Nakamura, E., Kobayashi, K., Tanaka, R., Kunihiro, T., Kitagawa, H. *et al.* (2022) On the origin and evolution of the asteroid Ryugu: A comprehensive geochemical perspective. *Proceedings of the Japan Academy, Series B* 98, 227–282. https://doi.org/10.2183/pjab.98.015

Nier, A.O. (1950) A Redetermination of the Relative Abundances of the Isotopes of Carbon, Nitrogen, Oxygen, Argon, and Potassium. *Physical Review* 77, 789–793. https://doi.org/10.1103/PhysRev.77.789

Okazaki, R., Marty, B., Busemann, H., Hashizume, K., Gilmour, J.D. *et al.* (2023) Noble gases and nitrogen in samples of asteroid Ryugu record its volatile sources and recent surface evolution. *Science* 379, eabo0431. https://doi.org/10.1126/science.abo0431

Ott, U. (2014) Planetary and pre-solar noble gases in meteorites. *Chemie der Erde* 74, 519–544. https://doi.org/10.1016/j.chemer.2014.01.003

Patzek, M., Kadlag, Y., Rüfenacht, M., Füri, E., Pack, A., Bischoff, A., Becker, H., Visser, R., John, T., Schönbächler, M. (2025) Multi-isotope (N, O, Ti, and Cr) study of C1 and CM-like clasts—Probing unsampled C1 material. *Meteoritics & Planetary Science* 60, 1073–1094. https://doi.org/10.1111/maps.14343

Pearson, V.K., Sephton, M.A., Franchi, I.A., Gibson, J.M., Gilmour, I. (2006) Carbon and nitrogen in carbonaceous chondrites: Elemental abundances and stable isotopic compositions. *Meteoritics & Planetary Science* 41, 1899–1918. https://doi.org/10.1111/j.1945-5100.2006.tb00459.x

Schultz, L., Franke, L. (2004) Helium, neon, and argon in meteorites: A data collection. *Meteoritics & Planetary Science* 39, 1889–1890. https://doi.org/10.1111/j.1945-5100.2004.tb00083.x

Vacher, L.G., Piani, L., Rigaudier, T., Thomassin, D., Florin, G., Piralla, M., Marrocchi, Y. (2020) Hydrogen in chondrites: Influence of parent body alteration and atmospheric contamination on primordial components. *Geochimica et Cosmochimica Acta* 281, 53–66. https://doi.org/10.1016/j.gca.2020.05.007

Yokoyama, T., Nagashima, K., Nakai, I., Young, E.D., Abe, Y. *et al.* (2023) Samples returned from the asteroid Ryugu are similar to Ivuna-type carbonaceous meteorites. *Science* 379, eabn7850. https://doi.org/10.1126/science.abn7850

Zimmermann, L., Füri, E. (2015) Ultra-high vacuum noble gas purification. Purification system. *Techniques de l'Ingénieur* J6634 V1.

Zimmermann, L., Füri, E., Burnard, P. (2015) Ultra-high vacuum noble gas purification. Purification methods. *Techniques de l'Ingénieur* J6635 V1.

Zimmermann, L., Füri, E., Boulliung, J., Saxton, J.M. (2025) Performance of the 3F4M Noblesse–HR noble gas mass spectrometer for multicollection Ne-Ar-N_2 analyses. *Geochemistry, Geophysics, Geosystems* 26, e2025GC012247. https://doi.org/10.1029/2025GC012247